S. GOLAK*, R. PRZYLUCKI*, J. BARGLIK*

DETERMINATION OF A MASS TRANSFER AREA DURING METAL MELTING IN A VACUUM INDUCTION FURNACE

OKREŚLENIE POWIERZCHNI WYMIANY MASY W PROCESIE WYTOPU METALI W INDUKCYJNYM PIECU PRÓŻNIOWYM

In the paper, a simulation model that allows for determination of the actual surface area of inductively stirred liquid metal and the value of metal near-surface velocity during its melting is presented. Also, the effects of induction furnace working frequency on both parameters are demonstrated. The simulation was performed for copper and liquid steel that were melted in two different induction furnaces. The calculation results were also used for determination of coefficients of copper mass transfer in liquid steel and of antimony mass transfer in liquid copper during their stirring in the discussed furnace.

Keywords: magnetohydrodynamics, free surface, mass transfer, numerical modelling

W pracy przedstawiono model symulacyjny pozwalający na wyznaczenie wartości rzeczywistej powierzchni ciekłego metalu mieszanego indukcyjnie jak i wartości prędkości przypowierzchniowej metalu w trakcie jego topienia. Wykazano jednocześnie wpływ częstotliwości roboczej pieca indukcyjnego na obydwie wielkości. Symulacji dokonano dla miedzi i ciekłej stali topionych w dwóch różnych piecach indukcyjnych. Wyniki obliczeń posłużyły także do wyznaczenia wartości współczynników transportu masy miedzi w ciekłej stali i antymonu w ciekłej miedzi w przypadku ich mieszania w omawianym agregacie.

1. Introduction

In many modern extraction metallurgy processes, a lot of heterogeneous reactions occur, most commonly in the liquid metal – gaseous phase, liquid slag – gaseous phase or solid phase – gaseous phase systems. Reactions of metal oxide reduction, metal refining by barbotage with gases or vacuum metal refining are examples of these processes. In the case of heterogeneous reactions, substances in particular phases can only react with each other when they reach the interface. For many processes, it is the surface of liquid metal or alloy. In general, the rate of mass flow from phase I to phase II resulting from the heterogeneous reaction can be determined as follows [1]:

$$N = k \cdot F \cdot \Delta\pi \tag{1}$$

where: k – overall mass transfer coefficient; F – interface area; $\Delta\pi$ – drive module.

Eq. (1) shows that the rate of heterogeneous reaction is directly proportional to the interface area. Therefore, modern technologies of metal production and metal refining aim at a wide expansion of this area. Moreover, its proper determination may clearly affect results of the kinetic analysis of these processes. This will be demonstrated with an example of vacuum metal refining where impurities evaporate from a bath of greater pressure than that of the primary metal. To determine the overall mass transfer coefficient for the evaporating com-

ponent based on the experimental data, the process rate may be described using the following equation [2]:

$$2.303 \cdot \log \frac{C^t}{C^o} = -k \cdot \frac{F}{V} t \tag{2}$$

where: V – liquid metal volume; t – process duration; C^t, C^0 – final and initial concentrations of the evaporating component, respectively.

In the above equation, a parameter that affects the value of overall mass transfer coefficient is also the interface area. Additionally, for the refining process conducted in the induction furnace, this parameter also influences the coefficient of mass transfer in the liquid phase, which is determined by the following equation [3]:

$$\beta^l = \left(\frac{8D \cdot v_s}{\pi \cdot r_m} \right)^{\frac{1}{2}} \tag{3}$$

where: v_s – near-surface velocity of inductively stirred liquid metal; r_m – radius of the liquid metal surface (assumed to be the melting pot inner radius); D – diffusion coefficient for the liquid alloy evaporating component.

Based on Eq. (3), it is shown that for the β^l estimation, the actual interface area and the near-surface velocity of liquid metal must be known. Considering the importance of interface area in the processes of metal melting and refining, a method for determination of liquid metal area in the induction furnace, with an example of copper alloys and liquid steel, is discussed.

* SILESIAN UNIVERSITY OF TECHNOLOGY, FACULTY OF MATERIALS ENGINEERING AND METALLURGY, 8 KRASINSKIEGO STR., 40-019 KATOWICE, POLAND

2. Numerical simulation methodology

So far, a lot of different models of crucible furnace for metal melting have been developed [4-6]. However, numerical modelling of molten metal bath treatment with the use of EM field, where near-surface phenomena are of critical importance [7], requires consideration of a change in the bath meniscus shape and a change in the meniscus influence on the EM field distribution. In such a case, the fundamental problem regarding numerical simulation is the necessity of strong coupling between electromagnetic field and flow field. In the coupling between fields, a changing (due to electromagnetic forces) shape of the liquid charge should also be considered [8-11]. The final shape of meniscus obtained in simulation is a result of a balance between electromagnetic forces, gravitational force, contact angle of crucible and molten metal as well as surface tension.

The first stage of simulation process was determination of the base liquid metal shape geometry. The geometry is an input for the electromagnetic field analysis calculations. For this stage of calculation, the Ansys Classic commercial software was used.

The hydrodynamic stage of simulation was conducted with the use of commercial software Ansys Fluent based on the finite volume formulation of Navier-Stokes equations. The formulation was supplemented with the k-epsilon turbulence model and source term of volumetric density of electromagnetic forces acting on the metal. Adoption of the finite volume method (VOF [12]) completes the momentum equation and mass conservation equation with the continuity equation taking into account a liquid phase presence.

After determination of the molten metal shape and velocity distribution in the Fluent program, it was necessary to determine modified molten metal shape geometry for electromagnetic field calculations with the use of the Ansys Classic. First, a set of cells with the edge of liquid metal was determined. Conditions for the cell to be considered an edge cell were as follows: the metal phase fraction greater than zero ($\alpha > 0$) and neighbourhood in one of four main directions (up, down, left, right) of the cell of a zero metal phase ($\alpha = 0$) or neighbourhood of the crucible wall.

After determination of the cells with the edge of liquid metal, a boundary of liquid metal was reconstructed in each cell in a simplified way (Fig. 2). It was made based on the metal phase fraction and its gradient (indicating a vertical or horizontal cell filling direction). In the centre of liquid metal edge, a point was determined which was a baseline point for the liquid metal geometry description in the Ansys Classic. For the cells partially filled with metal ($0<\alpha<1$), adjoining the crucible wall, a line passing through the two adjacent points was projected on the cell edge and in this way, an additional point was obtained. In the case of a corner cell, its vertex became another point of the Ansys Classic geometry description. For the cells entirely filled with metal ($\alpha =1$), centres of their edges, adjoining the crucible wall, determined next geometry points. Because only quadrilateral cells of the size significantly smaller than the calculation area were used in the hydrodynamic model, this simple (compared with other algorithms [11]) method of geometry reconstruction was precise enough to describe the geometry for electromagnetic calculations.

Direct transfer of geometry from the Fluent to the Ansys Classic is not recommended because of differences in mesh discretisation for electromagnetic and flow field analysis. For this reason, development of filtration algorithm to leave only significant points from among all points in the list was necessary. A flowchart of this algorithm is presented in Fig. 3. The processed input point list (from the stage presented in Fig. 2) was looped, i.e. the last point in the list preceded the first one. The threshold value, representing deviation of the part of the edge line from the straight line used in the algorithm, expressed the precision of geometry mapping. In the performed simulations, experimental adoption of 2 mm as a threshold value ensured good mapping of metal meniscus shape with the use of a dozen points.
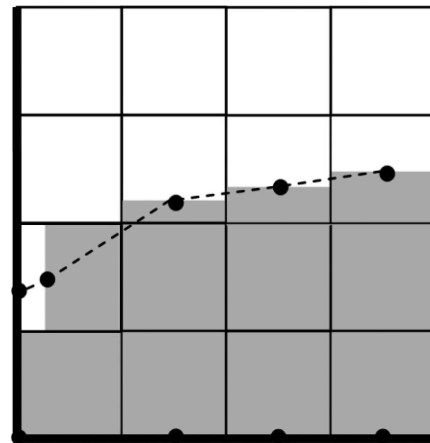

Fig. 2. Metal – environment boundary location in the edge cells with points describing metal charge

On determination of the list of distinctive points of metal shape geometry, its values were transferred to the Ansys Classic program where, after supplementation with the inductor geometry, the entire model was meshed with the use of triangular elements. After discretisation, equations describing the E-M field were solved. In the considered case, the EM field analysis was based on the Maxwell equation formulated with the use of magnetic vector potential. Distribution of elec-

Fig. 1. Determination of cells with the edge of molten metal (bold marks denote edge cells)

tromagnetic forces calculated in the Ansys Classic program was transferred back to the Fluent where the electromagnetic forces became the source term in the momentum equation. The use of entirely different kind of discretisation meshes for fluid dynamic calculations (quadrilateral) and for electromagnetic field analysis (triangular) as well as the use of different numerical methods applied for the Maxwell equation solution (based on the mesh nodes) and the Navier – Stokes (based on the cell centre – FVM) solution forced the necessity of interpolation of the electromagnetic forces distribution during their transfer to the fluid dynamic calculation model. To do this, the weight average value, calculated on the basis of values from three nodes of EM mesh located near the centre point of the cell from the fluid calculation mesh, was used. The weight coefficients were proportional to the distance between the node from EM mesh and the centre point of the fluid calculation mesh.
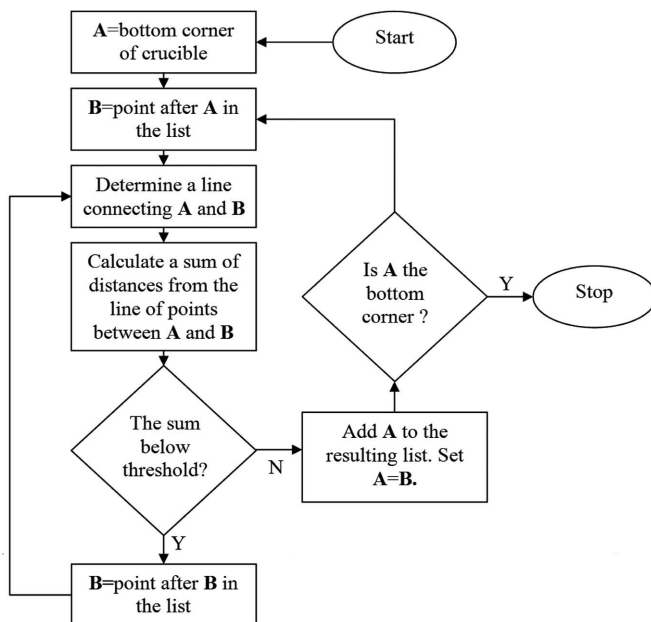

Fig. 3. Algorithm of choice of representative points for metal charge geometry description

The fluid dynamic calculations, including distribution of electromagnetic forces acting on the metal bath, allowed for determining actual distribution of the velocity field and the shape of free surface of the metal. The shape of metal was again approximated and transferred to the Ansys Classic program, which began the next simulation cycle for the next time step.

A condition for calculation completion was stabilisation of the liquid metal velocity and stabilisation of the metal meniscus shape.

3. Numerical simulation results

On the basis of prescribed model, numerical simulations were performed for two units differing in the type of charge material, crucible's and inductor's geometries as well as in the electromagnetic field frequency. The first unit was used for copper melting. Its schematic diagram is presented in Fig. 4a.

The metal was melted in a typical conical crucible placed inside a cylindrical inductor supplied with the current of 3.4 kA and 3 kHz. In Fig. 5a and 5b, distribution and values of the electromagnetic forces acting on the molten metal, at the moment of power start-up, are presented, respectively.
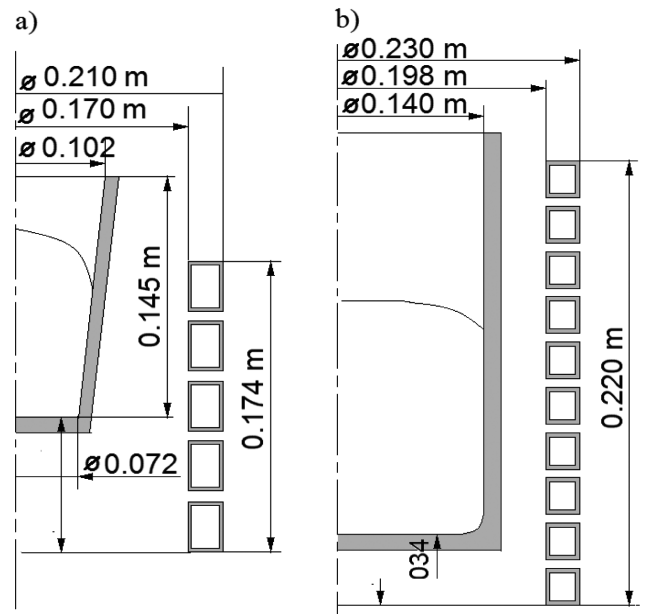

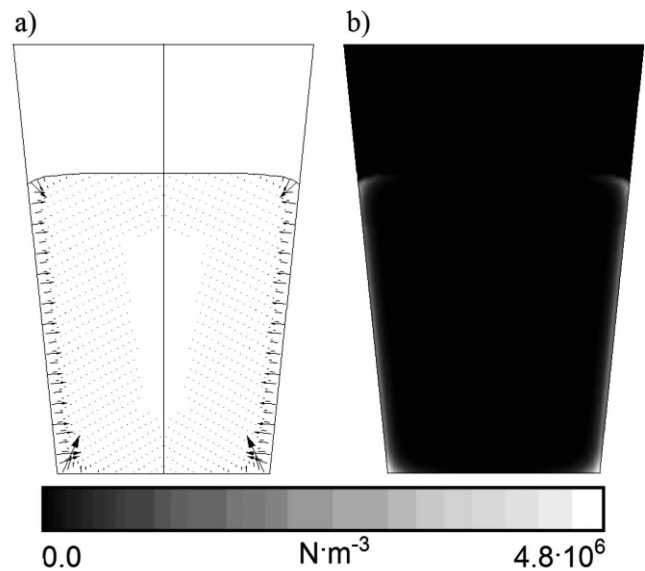Fig. 4. Geometry of the calculation units: a – for the copper charge, b – for the steel charge

Fig. 5. Distribution of electromagnetic forces acting on the molten copper: a – shape of the molten metal and vector representation of the forces, b – values

As shown in Fig. 5, the distribution of electromagnetic forces is characterised by considerable non-uniformity, which results in forcing of metal flow [13]. Additionally, high values of compressing forces appearing in the upper part of the molten metal result in strong deformation of the metal surface. As a result, the initial meniscus, which is merely a result of the crucible wetting with the metal as well as metal surface tension, will significantly increase. In Fig. 6, a final shape of the meniscus and velocity distribution in the molten metal in

a steady state are presented. The change of meniscus shape caused a 45% increase in the liquid metal surface area, which has a significant effect on all processes related to the surface area value.
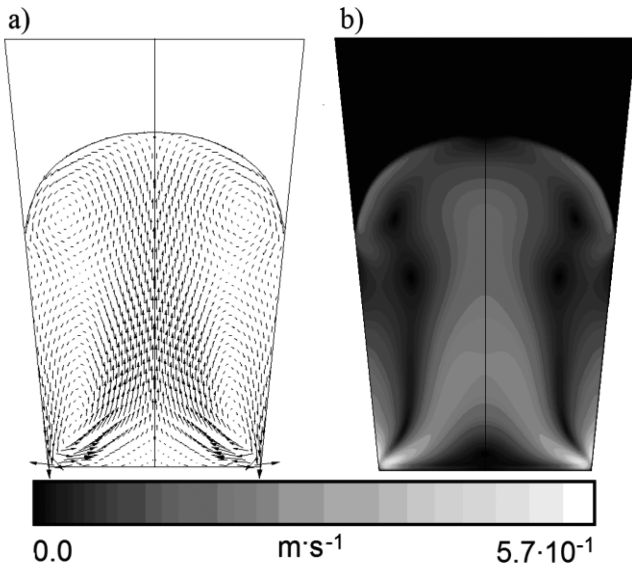

Fig. 6. Distribution of velocity in the molten copper: a – shape of the molten metal and vector representation of the velocity, b – velocity values

Using the velocity distribution, an average velocity value, 0.103 m/s, and an average value of the near-surface velocity, 0.129 m/s, were determined. These values are suggestive of intense stirring of the molten metal. The velocity values obtained in the near-surface region are significantly higher than the average velocity in the whole molten metal.

The shape of meniscus, determined from the simulation, is significantly different from the "natural" meniscus. Such differences were observed during actual work of the unit.
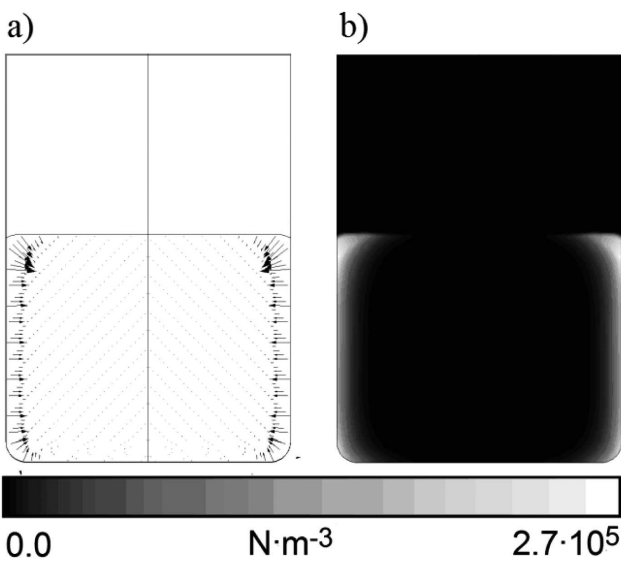

Fig. 7. Distribution of electromagnetic forces acting on the molten steel: a – shape of the molten metal and vector representation of the forces, b – values
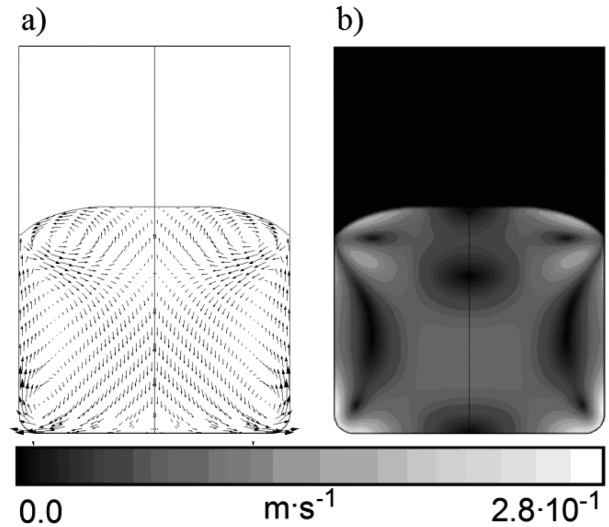

Fig. 8. Distribution of velocity in the molten steel: a – shape of the molten metal and vector representation of the velocity, b – velocity values

In the second part of the numerical experiment, steel was melted in the other unit (Fig. 4b) which was a ceramic, non-conductive cylindrical crucible. Its schematic diagram is presented in Fig. 4b. For this experiment, inductor's supply current intensity was 0.74 kA and its frequency was 5 kHz. Distribution of the electromagnetic forces acting on molten steel, at the moment of power start-up, is presented in Fig. 7, and distribution of velocity vectors, for the meniscus in the steady state, is shown in Fig. 8. For the steel processing unit, a significant increase in the surface area also occurred. In this case, the surface increase due to electromagnetic forces was about 9.5%. The average values of liquid metal velocity in the whole metal volume and in the near-surface area were 0.073 m/s and 0.113 m/s, respectively.

4. Influence of supply frequency on the meniscus and the velocity distribution field

Nominal supply frequencies for the units under consideration were 3 and 5 kHz, respectively. As the frequency of applied electromagnetic field significantly affects the electromagnetic field depth of penetration and, therefore, distribution of electromagnetic forces acting on the molten metal, the velocity distribution and meniscus shape are strongly dependent on the supply frequency.

In Fig. 9, the surface area, average near-surface velocity of liquid copper and average velocity in the whole liquid copper bath versus the frequency are presented.
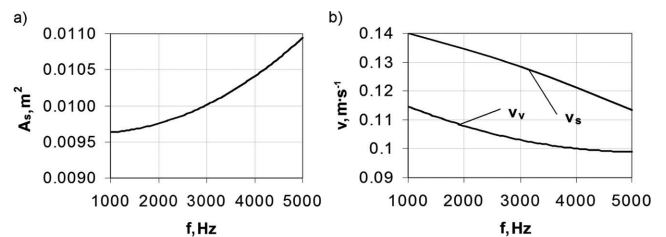

Fig. 9. Copper surface area (a) and velocity (b) versus frequency for the supply current intensity of 3.4 kA; v_v – whole volume average velocity, v_s – subsurface velocity

As shown in Fig. 9, increased supply frequency increases the surface deformation, and thus the surface area. This is due to higher values of compressive forces acting on the liquid metal, while the inductor supply current had the same value of 3.4 kA. It would suggest the increase in efficiency of processes occurring on the liquid metal – ambient environment interface. However, at the same time, the frequency increase causes reduction in the velocity of liquid metal movements, the average velocity and near-surface velocity, which results in less intense transfer of the components to the surface area.
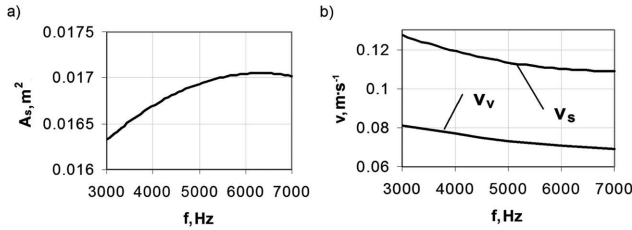
Fig. 10. Steel surface area (a) and velocity (b) versus the frequency for the supply current intensity of 3.4 kA; v_v – whole volume average velocity, v_s – subsurface velocity

A similar dependency can be observed for the second unit intended for steel processing. Results obtained for this case are presented in Fig. 10. Here (for steel and the cylindrical crucible), two opposing phenomena can also be observed: increased surface area of the liquid metal but reduced velocity of liquid metal movement, which results in smaller efficiency of transfer of the reactants to the surface area.

5. Analysis of results

Based on the results of performed simulations, values of the coefficient of mass transfer in the liquid phase were estimated for copper alloy and steel melting processes. The results were compared to the literature data obtained by the authors of papers [14, 15] who investigated elimination of antimony from liquid copper and elimination of copper from liquid steel during the processes conducted in the induction furnace. The obtained results are presented in Tables 1-2 and Fig. 11-12. The values of β^l_{Fe} and β^l_{Cu} coefficients were determined using the equation (3), assuming that the actual mass transfer area was equal to the inner surface area of the crucible. The values of β^{l*}_{Fe} and β^{l*}_{Cu} coefficients were also determined using the equation (3) as well as the value of liquid metal surface area determined based on the proposed numerical simulation. Both for liquid steel and copper, the β^l_{Fe} and β^l_{Cu} coefficients were greater than the values of β^{l*}_{Fe} and β^{l*}_{Cu} by up to 10%.

TABLE 1

Values of mass transfer coefficient in the liquid phase for VIM steel

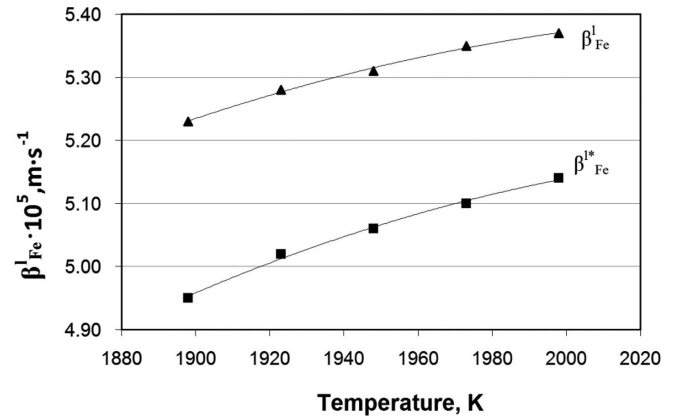| Temperature, K	1898	1923	1948	1973	1998
Coefficient $\beta^l_{Fe} \cdot 10^5, m \cdot s^{-1}$	5.23	5.28	5.31	5.35	5.37
Coefficient $\beta^{l*}_{Fe} \cdot 10^5, m \cdot s^{-1}$	4.95	5.02	5.06	5.10	5.14

Fig. 11. Determined values of coefficients of mass transfer in the liquid phase for inductively stirred steel

TABLE 2

Values of mass transfer coefficient in the liquid phase for VIM copper

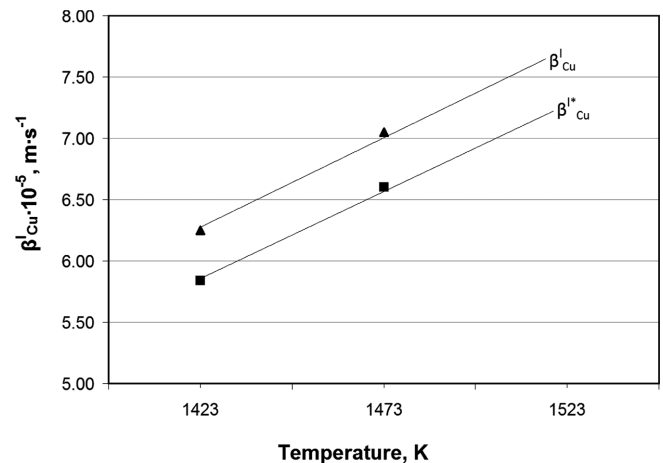| Temperature, K	1423	1473	1523
Coefficient $\beta^l_{Cu} \cdot 10^5, m \cdot s^{-1}$	6.25	7.05	7.71
Coefficient $\beta^{l*}_{Cu} \cdot 10^5, m \cdot s^{-1}$	5.84	6.60	7.26

Fig. 12. Determined values of coefficients of mass transfer in the liquid phase for inductively stirred copper

6. Summary

The proposed simulation model allowed for determination of both the actual surface area of liquid metal and the value of near-surface velocity of inductively stirred metal. Also, the effects of induction furnace working frequency on both parameters were demonstrated. The simulation was performed for copper and liquid steel that were melted in two different induction furnaces. The calculation results were also used for determination of coefficients of copper mass transfer in liquid steel and of antimony mass transfer in liquid copper. The obtained coefficients differ from the literature data as during determination of the latter values, the meniscus phenomenon that occurs during metal induction melting was not considered.

REFERENCES

[1] L. B l a c h a, Arch. Metall. **48** (1), 105-127 (2003).

[2] L. B l a c h a, F. M i z e r a, P. F o l e g a, Metalurgija **53** (4), 51-54 (2014).

[3] G. S i w i e c, Arch. Metall. Mater. **58** (4), 1155-1160 (2013).

[4] M. S c e p a n s k i s, A. J a k o v i c s, E. B a a k e, B. N a c k e, Magnetohydrodynamics **48** (4), 677-686 (2012).

[5] R. S c h w a r z e, F. O b e r m e i e r, Model. Simul. Mater. Sc. **12** (5), 985-993 (2004).

[6] A. B e r m u d e z, D. G o m e z, M. M u n i z, P. S a l g a d o, R. V a z q u e z, Appl. Numer. Math. **59** (9), 2082-2104 (2009).

[7] L. B l a c h a, R. B u r d z i k, A. S m a l c e r z, T. M a t u l a, Arch. Metall. Mater. **58** (1), 197-201 (2013).

[8] S. G o l a k, R. P r z y l u c k i, A simulation of the coupled problem of magnetohydrodynamics and a free surface for liquid metals, Transactions on Engineering Science, WIT, 67-76 (2009).

[9] S. G o l a k, R. P r z y l u c k i, Prz. Elektrotechniczn. **84** (11), 163-164 (2008).

[10] S. S p i t a n s, A. J a k o v i c s, E. B a a k e, B. N a c k e, Metall. Mater. Trans. B **44** (3), 593-605 (2013).

[11] O. P e s t e a n u, E. B a k k e, ISIJ Int. **51** (5), 707-713 (2011).

[12] C.W. H i r t, B.D. N i c h o l s, J. Comput. Phys. **39** (1), 201-225 (1981).

[13] S. G o l a k, R. P r z y l u c k i, IEEE T. Magn. **47** (12), 4701-4706 (2011).

[14] L. B l a c h a, Arch. Metall. Mater. **50** (4), 989-1002 (2005).

[15] J. L a b a j, Arch. Metall. Mater. **57** (1), 165-172 (2012).